

# Electrohydrodynamic interactions of drop pairs

Chiara Sorgentone<sup>1</sup> and Petia M. Vlahovska<sup>2</sup>

<sup>1</sup> KTH Mathematics, Linné Flow Centre, 10044 Stockholm, Sweden

<sup>2</sup> Engineering Sciences and Applied Mathematics, Northwestern University, Evanston, IL 60208, USA

(Received 30 May 2022)

We present three-dimensional simulations of the dynamics of a drop pair in an applied uniform DC electric field. The numerical method is based on a boundary integral formulation of the leaky dielectric model. We apply the method to explore the electrohydrodynamic interactions between two identical drops with arbitrary orientation of their line of centers relative to the applied field direction. Our results show complex dynamics depending on the conductivities and permittivities of the drops and suspending fluids, and the drop pair alignment with the applied electric field.

## 1. Introduction

The interaction of fluids and electric fields is at the heart of natural phenomena such as the disintegration of raindrops in thunderstorms and many practical applications such as electrosprays (Ganan-Calvo *et al.* 2016), microfluidics (Stone *et al.* 2005), and crude oil demulsification (Eow & Ghadiri 2002). Many of these processes involve drops and there has been growing interest in understanding the drop-drop dynamics of in the presence of electric field.

A drop placed in an electric field polarizes, if its permittivity and/or conductivity are different than the suspending fluid. The polarization leads to a jump in the electric stresses across the drop interface. In the case of fluids that are perfect dielectrics, only the normal electric stress is discontinuous at the interface. If the electric pressure can be balanced by surface tension, the drop adopts a steady prolate shape and the fluids are quiescent. The physical picture changes dramatically if the fluids are leaky dielectrics. Finite conductivity enables the passage of electric current and electrical charge accumulates at the drop interface. The electric field acting on this induced surface charge creates tangential electric stress, which shears the fluids into motion. The complicated interplay between the electrostatic and viscous fluid stresses results in either oblate or prolate drop deformation in weak fields (Taylor 1966), and complex dynamics in strong fields, such as break-up (Lac & Homsy 2007; Karyappa *et al.* 2014), streaming either from the drop poles (de la Mora 2007; Collins *et al.* 2013, 2008; Sengupta *et al.* 2017) or equator (Brosseau & Vlahovska 2017), and electrorotation (Ha & Yang 2000; Salipante & Vlahovska 2010, 2013).

While the prototypical problem of an isolated drop in a uniform electric field has been extensively studied (see for a recent review (Vlahovska 2019)), investigations of the collective dynamics of many drops are scarce (Casas *et al.* 2019) and mainly focused on the near-contact interaction preceding electrocoalescence (Anand *et al.* 2019; Roy *et al.* 2019). The dynamics drop approach and interactions at arbitrary separations have been considered mainly in the case of droplet pairs aligned with the electric field (Baygents

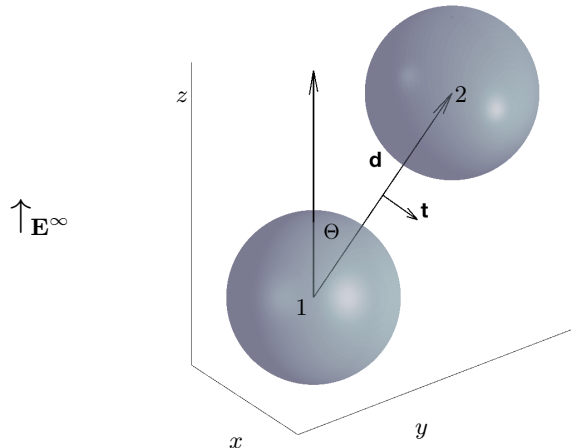


FIGURE 1. Two initially spherical identical drops with the same radius  $a$ , permittivity  $\varepsilon_d$  and conductivity  $\sigma_d$  suspended in a fluid permittivity  $\varepsilon_s$  and conductivity  $\sigma_s$  and subjected to a uniform DC electric field  $\mathbf{E}^\infty = E_0 \hat{\mathbf{z}}$ .

*et al.* 1998; Lin *et al.* 2012; Mhatre *et al.* 2015; Zabarankin 2020), because the axial symmetry greatly simplifies the calculations. These studies revealed that in leaky dielectric systems the hydrodynamics interactions due to the electric-shear-driven flow can play a significant role. For example, in the case of a drop with drop-medium ratio of conductivities  $R$  and permittivities  $S$  such that  $R/S > 1$ , the electrohydrodynamic flow generates repulsion which opposes the electrostatic attraction due to the drop dipoles and the drops move apart.

The general case of an electric field applied at an angle to the line joining the centers of the two drops is studied only to a limited extent experimentally (Mhatre *et al.* 2015) and via numerical simulations in two dimensions (Dong & Sau 2018). This configuration has been systematically analyzed only for a pair of non-deformable, ideally polarizable spheres (Saintillan 2008). In this case, the flow about the spheres, due to induced charge electrophoresis, has the same stresslet-quadrupole structure as the electrohydrodynamic flow about a drop with  $R/S < 1$ . The study showed that the pair dynamics is not simple attraction or repulsion; depending on the angle between the center-to-center line with the undisturbed electric field, the relative motion of the two spheres can be quite complex: they attract in the direction of the field and move towards each other, pair up, and then separate in the transverse direction. To the best of our knowledge, such dynamics in the case of drops has not been reported. Motivated by the observed intricate trajectories of ideally polarizable spheres and the similarities in their electrohydrodynamic interactions with the drops with  $R/S < 1$ , we set up to investigate the effects of drop electric properties (conductivity ratio  $R$  and permittivity ratio  $S$ ) and deformability on the relative motion of a drop pair initially misaligned with the applied field.

## 2. Problem formulation

Let us consider two identical neutrally-buoyant and charge-free drops with same radius  $a$  and same conductivity  $\sigma_d$  and permittivity  $\varepsilon_d$ , suspended in a fluid with conductivity  $\sigma_s$ , and permittivity  $\varepsilon_s$ . The mismatch in drop and suspending fluids electric properties is characterized by the conductivity and permittivity ratios,

$$R = \frac{\sigma_d}{\sigma_s}, \quad S = \frac{\varepsilon_d}{\varepsilon_s}. \quad (2.1)$$

In general, the drop and the suspending fluids have different viscosities  $\eta_d$  and  $\eta_s$ , respectively. In this study, we assume all fluids to have same viscosity, i.e., the viscosity ratio  $\lambda = \eta_d/\eta_s = 1$ . The unit separation vector between the drops is defined by the difference between the position vectors of the drops centers of mass  $\hat{\mathbf{d}} = (\mathbf{x}_2^c - \mathbf{x}_1^c)/d$ . The problem geometry is sketched in Figure 1.

### 2.1. Governing equations and numerical method

We adopt the leaky dielectric model (Melcher & Taylor 1969; Saville 1997; Vlahovska 2019), which assumes creeping flow and charge-free bulk fluids acting as Ohmic conductors. The electric field is irrotational, and Gauss' law dictates that the electric field  $\mathbf{E}$  in the drop and suspending fluids is solenoidal

$$\nabla \cdot \mathbf{E}^d = 0, \quad \nabla \cdot \mathbf{E}^s = 0. \quad (2.2)$$

At the drop interfaces  $\mathcal{D}$ , the normal electric current and tangential electric field are continuous

$$\sigma_s E_n^s = \sigma_d E_n^d, \quad \mathbf{E}_t^d = \mathbf{E}_t^s, \quad \mathbf{x} \in \mathcal{D} \quad (2.3)$$

where  $E_n = \mathbf{E} \cdot \mathbf{n}$ ,  $\mathbf{E}_t = \mathbf{E} - E_n \mathbf{n}$ , and  $\mathbf{n}$  is the outward pointing normal vector to the drop interface. Far away from the drops,  $\mathbf{E}^s \rightarrow \mathbf{E}^\infty = E_0 \hat{\mathbf{z}}$ .

Fluid motion is described by the Stokes equations. The velocity,  $\mathbf{u}$ , and dynamic pressure,  $p$ , in each fluid phase satisfy

$$\eta \nabla^2 \mathbf{u} = \nabla p, \quad \nabla \cdot \mathbf{u} = 0. \quad (2.4)$$

The assumption of charge-free fluids decouples the electric and hydrodynamic fields in the bulk. The coupling occurs at the drop interfaces, through the boundary conditions for mechanical equilibrium. The hydrodynamic and electric tractions at the interface are discontinuous and balanced by the capillary stress due to curvature along the drop interface

$$\mathbf{n} \cdot [(\mathbf{T}^s - \mathbf{T}^d) + (\mathbf{T}^{s,el} - \mathbf{T}^{d,el})] = \gamma \mathbf{n} (\nabla \cdot \mathbf{n}), \quad \mathbf{x} \in \mathcal{D}, \quad (2.5)$$

where  $\gamma$  is the interfacial tension.  $T_{ij} = -p\delta_{ij} + \eta(\partial_j u_i + \partial_i u_j)$  is the hydrodynamic stress and  $\delta_{ij}$  is the Kronecker delta function. The electric stress is given by the Maxwell stress tensor  $T_{ij}^{el} = \varepsilon (E_i E_j - E_k E_k \delta_{ij}/2)$ .

Henceforth, all variables are nondimensionalized using the radius of the undeformed drops  $a$ , the undisturbed field strength  $E_0$ , a characteristic applied stress  $\tau_c = \varepsilon_s E_0^2$ , and the properties of the suspending fluid. Accordingly, the time scale is  $t_c = \eta/\tau_c$  and the velocity scale is  $u_c = a\tau_c/\eta_s$ .

We utilize the boundary integral method to solve for the flow and electric fields. Details of our three-dimensional formulation can be found in (Sorgentone *et al.* 2019). In brief,

the electric field is computed following (Lac & Homay 2007; Baygents *et al.* 1998):

$$\mathbf{E}^\infty - \sum_{j=1}^2 \int_{\mathcal{D}_j} \frac{\hat{\mathbf{x}}}{4\pi r^3} (\mathbf{E}^s - \mathbf{E}^d) \cdot \mathbf{n} dS(\mathbf{y}) = \begin{cases} \mathbf{E}^d(\mathbf{x}) & \text{if } \mathbf{x} \text{ inside } \mathcal{D}, \\ \frac{1}{2} (\mathbf{E}^d(\mathbf{x}) + \mathbf{E}^s(\mathbf{x})) & \text{if } \mathbf{x} \in \mathcal{D}, \\ \mathbf{E}^s(\mathbf{x}) & \text{if } \mathbf{x} \text{ outside } \mathcal{D}. \end{cases} \quad (2.6)$$

where  $\hat{\mathbf{x}} = \mathbf{x} - \mathbf{y}$  and  $r = |\hat{\mathbf{x}}|$ . The normal and tangential components of the electric field are calculated from the above equation

$$\begin{aligned} E_n(\mathbf{x}) &= \frac{2R}{R+1} \mathbf{E}^\infty \cdot \mathbf{n} + \frac{R-1}{R+1} \sum_{j=1}^2 \int_{\mathcal{D}_j} \frac{\hat{\mathbf{x}} \cdot \mathbf{n}}{2\pi r^3} E_n(\mathbf{y}) dS(\mathbf{y}), \\ \mathbf{E}_t(\mathbf{x}) &= \frac{\mathbf{E}^s + \mathbf{E}^d}{2} - \frac{1+R}{2R} E_n \mathbf{n}. \end{aligned} \quad (2.7)$$

For the flow field, we have developed the method for fluids of arbitrary viscosity, but for the sake of brevity here we list the equation in the case of equiviscous drops and suspending fluids. The velocity is given by

$$2\mathbf{u}(\mathbf{x}) = - \sum_{j=1}^2 \left( \frac{1}{4\pi} \int_{\mathcal{D}_j} \left( \frac{\mathbf{f}(\mathbf{y})}{Ca} - \mathbf{f}^E(\mathbf{y}) \right) \cdot \left( \frac{\mathbf{I}}{r} + \frac{\hat{\mathbf{x}}\hat{\mathbf{x}}}{r^3} \right) dS(\mathbf{y}) \right), \quad (2.8)$$

where  $\mathbf{f}$  and  $\mathbf{f}^E$  are the interfacial stresses due to surface tension and electric field

$$\mathbf{f} = \nabla \cdot \mathbf{n}, \quad \mathbf{f}^E = (\mathbf{E}^s \cdot \mathbf{n}) \mathbf{E}^s - \frac{1}{2} (\mathbf{E}^s \cdot \mathbf{E}^s) \mathbf{n} - S \left( (\mathbf{E}^d \cdot \mathbf{n}) \mathbf{E}^d - \frac{1}{2} (\mathbf{E}^d \cdot \mathbf{E}^d) \mathbf{n} \right). \quad (2.9)$$

The electric capillary number compares the magnitude of the electric stresses and surface tension

$$Ca = \frac{\varepsilon_s E_0^2 a}{\gamma} \quad (2.10)$$

To solve the system of equations Eq. (2.7) and Eq. (2.8) we use the boundary integral method presented in Sorgentone *et al.* (2019). All variables are expanded in spherical harmonics and special algorithms are designed to deal with singular and nearly singular quadratures, particularly important when dealing with multiple drops interacting. We also use the spectral reparametrization technique presented in Sorgentone & Tornberg (2018), designed to keep the representation optimal even under strong deformations. All details regarding the numerical method can be found in the cited papers, exception made for the time-stepper scheme that we updated for the present simulations to the adaptive fourth order Runge-Kutta presented in Kennedy & Carpenter (2003). In this work, we set the spherical harmonic expansion order to  $p = 9$  and the viscosity contrast is  $\lambda = 1$  (changing this parameter would only affects the time scale but not the qualitatively behaviour of the interaction). Unless otherwise explicitly stated, the electric capillary number is  $Ca = 0.1$ .

### 3. Results and discussion

An isolated charge-neutral drop in a uniform DC electric field experiences no net force. However, a drop pair can move due to their mutual electrostatic (due to the induced surface charge) and hydrodynamic (due to the flow driven by the surface electric shear) interactions.

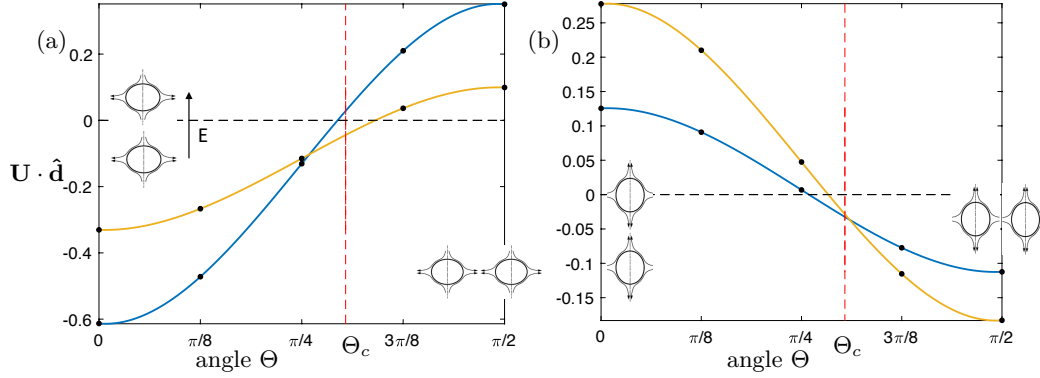


FIGURE 2. Radial component  $\mathbf{U} \cdot \hat{\mathbf{d}}$  of the relative velocity between the two drops  $\mathbf{U} = \mathbf{U}_2 - \mathbf{U}_1$  as a function of the angle made between the applied field and the line of centers of the two spheres  $\mathbf{E}^\infty \cdot \hat{\mathbf{d}} = \cos \Theta$ . Initial separation is  $d = 2.5$ . (a)  $R/S < 1$ :  $R = 2, S = 3$  (yellow),  $R = 0.1, S = 1$  (blue). At  $\Theta = 0$ , both electrostatic (DEP) and electrohydrodynamic (EHD) interactions are attractive. At  $\Theta = \frac{\pi}{2}$ , both DEP and EHD are repulsive. (b)  $R/S > 1$ :  $R = 2, S = 1$  (yellow),  $R = 2, S = 1/3$  (blue). At  $\Theta = 0$ , DEP is attractive and EHD is repulsive, while  $\Theta = \frac{\pi}{2}$  the interactions switch sign: DD is repulsive and EHD is attractive.

### 3.1. Far-field interactions

To gain more physical insight, it is instructive to analyze the interaction of two widely separated drops. In this case, the drops can be approximated by point-dipoles. The disturbance field  $\mathbf{E}_1$  of the drop dipole  $\mathbf{P}_1$  creates a dielectrophoretic (DEP) force on the dipole  $\mathbf{P}_2$  located at  $\mathbf{x}_2^c = d\hat{\mathbf{d}}$ ,  $\mathbf{F}(d) = (\mathbf{P}_2 \cdot \nabla \mathbf{E}_1)|_{r=d}$

$$\mathbf{F}(d) = \mathbf{P}_1 \mathbf{P}_2 : \nabla \left( \frac{\mathbf{I}}{r^3} - 3 \frac{\mathbf{xx}}{r^5} \right) \Big|_{r=d}, \quad \mathbf{P}_1 = \mathbf{P}_2 = \frac{R-1}{R+2} \mathbf{E}^\infty \quad (3.1)$$

The drop velocity under the action of this force can be estimated from Stokes law,  $\mathbf{U}_2 = -\mathbf{U}_1 = \mathbf{F}/\zeta$ , where  $\zeta$  is the friction coefficient,  $\zeta = 2\pi(3\lambda + 2)/(\lambda + 1)$ . The radial component of the force depends on the angle  $\Theta$  made between the direction of the external field and the line joining the centers of the two drops

$$\mathbf{F} \cdot \hat{\mathbf{d}} = \frac{D}{r^4} (1 - 3 \cos^2 \Theta), \quad D = 12\pi \left( \frac{R-1}{R+2} \right)^2 \quad (3.2)$$

It is attractive if  $\Theta < \Theta_c = \arccos\left(\frac{1}{\sqrt{3}}\right) \approx 54.7^\circ$ , e.g., when the drops are lined up with the field, and repulsive if the line of centers of the two drops is perpendicular to the field.

The electrohydrodynamic (EHD) flow about an isolated, spherical drop is a combination of a stresslet and a quadrupole. At the surface of the drop,

$$\mathbf{u}(r=1) = V \hat{\boldsymbol{\theta}}, \quad V = \frac{9}{10} \frac{R-S}{(1+\lambda)(R+2)^2}. \quad (3.3)$$

If  $R/S < 1$ , the surface flow is from pole to equator, i.e, fluid is drawn in at the poles and pushed away from the drop at the equator. The flow direction is reversed for  $R/S > 1$ . Away from the drop, the stresslet flow dominates due to its slower decay with the distance from the drop ( $\sim 1/r^2$ ) compared to the quadrupole flow ( $\sim 1/r^4$ ). The far-field EHD

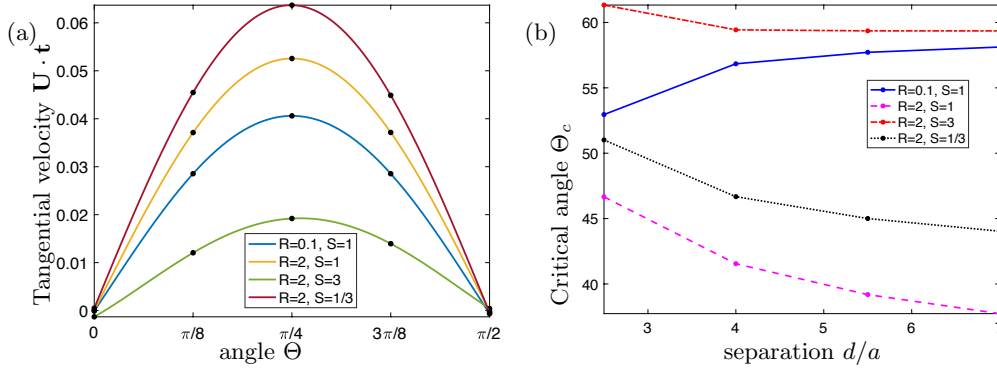


FIGURE 3. (a) Tangential component  $\mathbf{U} \cdot \hat{\mathbf{t}}$  of the relative velocity between the two drops  $\mathbf{U} = \mathbf{U}_2 - \mathbf{U}_1$  as a function of the angle made between the applied field and the line of centers of the two drops  $\mathbf{E}^\infty \cdot \hat{\mathbf{d}} = \cos \Theta$ . (b) Critical value of the angle  $\Theta$  for which the radial velocity between two spheres is zero, plotted as a function of the separation distance between the drops. This critical angle separates configurations for which drops attract ( $\mathbf{U} \cdot \hat{\mathbf{d}} < 0$ ) and repel ( $\mathbf{U} \cdot \hat{\mathbf{d}} > 0$ ). If  $R/S < 1$ , interaction is attractive for  $\Theta < \Theta_c$ , while for  $R/S > 1$ , interaction is attractive for  $\Theta > \Theta_c$ .

flow can be approximated by a stresslet with strength  $V\hat{\mathbf{z}}\hat{\mathbf{z}}$

$$\mathbf{u}_s(\mathbf{x}) = V(-1 + 3\cos^2\Theta)\frac{\mathbf{x}}{r^3} \quad (3.4)$$

A drop located at a distance  $d \gg 1$  and angle  $\Theta$  to a leading order moves with the velocity induced by the stresslet,  $\mathbf{U}_2 = -\mathbf{U}_1 = \mathbf{u}_s(d\hat{\mathbf{d}})$ . The electrohydrodynamic interaction depends on the sign of the induced free-charge dipole  $\sim (R - S)$ . If  $R/S < 1$ , the pole to equator flow pulls the drops together when lined parallel to the applied field direction and pushes them apart when the center-to-center line is perpendicular to the field (note that this scenario reverses for  $R/S > 1$ ). The critical angle which separates attraction from repulsion is the same as the dielectrophoretic force,  $\Theta_c \arccos\left(\frac{1}{\sqrt{3}}\right) \approx 54.7^\circ$ . Hence, to a leading order, both the DEP and EHD change sign at  $\Theta_c$ .

The initial interaction of two drops at different misalignment with the applied field is illustrated in Figure 2 and figure 3 by the dependence on  $\Theta$  of the initial relative velocity  $\mathbf{U} = \mathbf{U}_2 - \mathbf{U}_1$  of the two drops. Figure 2 shows that the radial component of the velocity changes sign. In the case  $R/S < 1$ , the electrostatic (DEP) and electrohydrodynamic (EHD) interactions work in the same direction. When the drop pair is aligned with the field ( $\Theta = 0$ ), the drops attract. As  $\Theta$  increases, the attraction decreases and changes to repulsion around  $\Theta \sim \Theta_c$ . The repulsion is strongest in the configuration with  $\Theta = \pi/2$ , i.e., line of drop centers perpendicular to the applied field. The critical angle at which the total interaction changes sign is close to the far-field result  $\Theta_c = 54.7^\circ$  and its dependence on the separation between the drops is shown in Figure 3b. In the far-field approximation, the tangential component of  $\mathbf{U}$  arises only from the electrostatic interaction,  $F_t = -D\sin(2\Theta)$ . Accordingly, it is maximal at  $\Theta = \pi/4$  as confirmed by Figure 3a. Purely dipolar interaction would result in drops “chaining”, i.e., drop aligning with the field, as the line of centers rotates with velocity  $U_t$ . Purely stresslet EHD interaction at leading order only results in attraction or repulsion along the line of centers, but no rotation of the drop pair.

While the behavior for drops with  $R/S < 1$  is in agreement with the predictions from

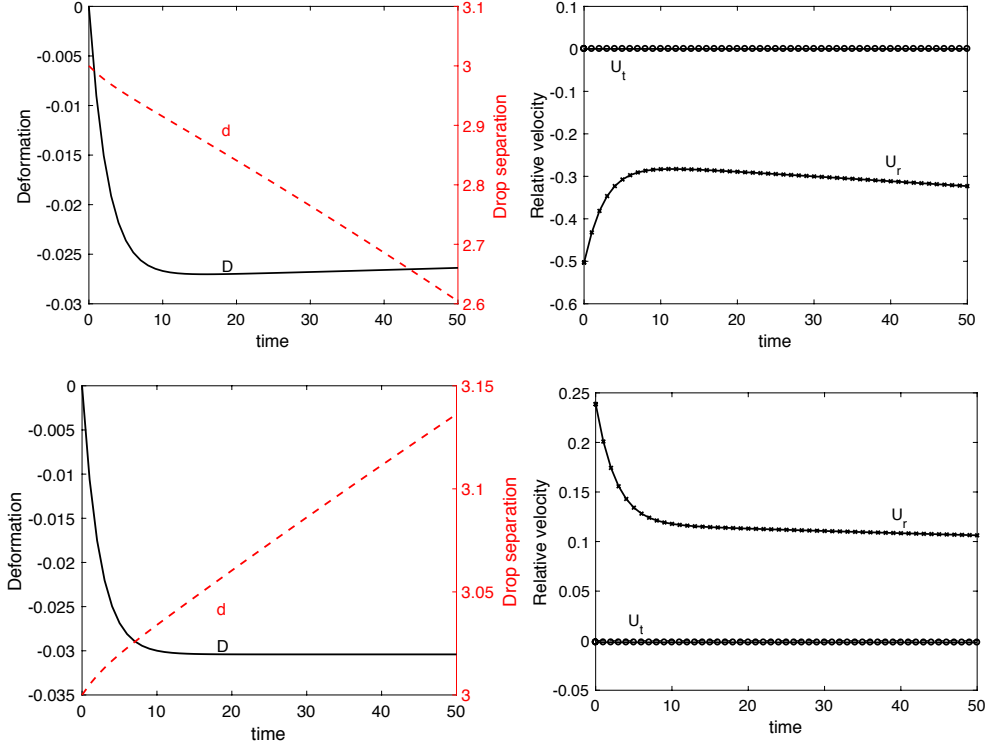


FIGURE 4. Electrohydrodynamics of a pair of deforming drops with  $R = 0.1$  and  $S = 1$  with initial separation  $d = 3$  and inclination  $\Theta = 0$  (top) and  $\Theta = \pi/2$  (bottom). Evolution of the radial and tangential components of the relative velocity, the deformation parameter and the center-to-center distance between the drops.

the point-dipole approximation, especially for the cross-over angle, the case  $R/S > 1$  is more complicated because the electrostatic (DEP) and electrohydrodynamic (EHD) interactions are antagonistic. EHD interactions based on the stresslet approximation are predicted to change from repulsive to attractive as  $\Theta$  increases, while the DEP follows the opposite trend. Figure 2b shows that for the considered cases the interaction is dominated by the EHD contribution. The reversal of the interaction sign as  $\Theta$  increases occurs at smaller angles compared to  $R/S < 1$ , likely due to the opposing effect of the DEP interaction. We have observed also that  $R = 3$ ,  $S = 1$  shows only attraction for all angles  $\Theta$  suggesting a complex dependence on the conductivity ratio  $R$ . Indeed, as  $R$  increases the EHD flow weakens (see Eq. (3.3)), while the DEP force plateaus as the dipole strength  $(R-1)/(R+2)$  approaches 1 as  $R \gg 1$  (see Eq. (3.2)). Hence, even though the EHD flow has a slower decay with separation  $d^{-2}$ , compared to DEP ( $\sim d^{-4}$ ), the weakening with increasing  $R$  may lead to the observed trend.

The question arises what happens after the initial attraction or repulsion? How does the deformation, hydrodynamic and electrostatic interactions affect the drop trajectory? Here we show that their interplay give rise to intricate trajectories. Next, we consider two identical drops and explore the effect of the initial configuration on the pair dynamics.

### 3.2. Arbitrary separations

Here we consider the full problem, i.e. the interaction between two deforming drops. Figures 4 and 5 illustrate the evolution of the radial and tangential components of the

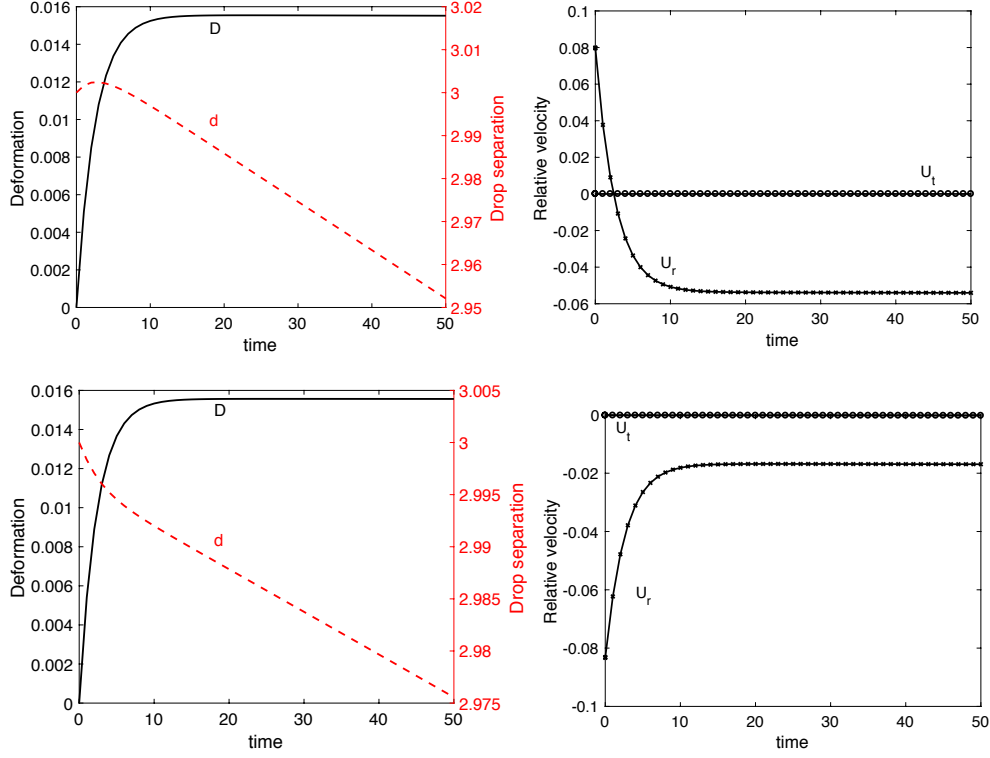


FIGURE 5. Electrohydrodynamics of a pair of deforming drops with  $R = 2$  and  $S = 1$  with initial separation  $d = 3$  and inclination  $\Theta = 0$  (top) and  $\Theta = \pi/2$  (bottom). Evolution of the radial and tangential distance components of the relative velocity, the deformation parameter and the center-to-center distance between the drops.

relative velocity, the deformation number of drop 1 and and the center-to-center distance between drops initially placed in the the two extreme configurations, aligned and perpendicular to the field,  $\Theta = 0$  and  $\Theta = \pi/2$ , respectively. The deformation parameter is defined as  $D_T = \frac{a_{||} - a_{\perp}}{a_{||} + a_{\perp}}$ , where  $a_{||}$  and  $a_{\perp}$  are the drop lengths in direction parallel and perpendicular to the applied field. For an isolated drop, in weak field ( $Ca \ll 1$ ) the equilibrium shape is given by

$$D_T = \frac{9Ca}{16(2+R)^2} \left[ R^2 + 1 - 2S + 3(R-S) \frac{2+3\lambda}{5(1+\lambda)} \right]. \quad (3.5)$$

Upon application of the field, the drop approaches the steady state monotonically

$$D(t) = D_T \left( 1 - e^{-t/t_r} \right) \quad \text{where} \quad t_r = \frac{\eta_s a}{\gamma} \left( \frac{(3+2\lambda)(16+19\lambda)}{40(1+\lambda)} \right). \quad (3.6)$$

Figures 4 and 5 show that upon application of the field the drops deform into an oblate for  $R/S < 1$  and prolate for  $R/S > 1$  ellipsoid. The deformation parameter increases monotonically, similarly to the isolated drop case, and approaches a nearly steady value, which is close to that for an isolated drop given by Eq. (3.5). In the axisymmetric case,  $\Theta = 0$ , the deformation parameters of both drops are identical. The difference with the isolated drop deformation is greater than the  $\Theta = \pi/2$  case because as the drops are



moving closer their interference is getting stronger; in the  $\Theta = \pi/2$  configuration, the drops move away from each other and become more isolated.

The tangential component of the relative velocity,  $U_t$ , is zero during the interaction and accordingly the drop pair orientation with the field remains unchanged, i.e., the angle between the line of centers remains as the initial configuration. The radial velocity,  $U_r = \mathbf{U} \cdot \hat{\mathbf{d}}$ , however varies in time and in most cases does not change sign (it remains either negative, indicating attraction, or positive, indicating attraction). In the case  $R/S < 1$  (Figure 4), in the  $\Theta = 0$  drops attract and the distance between the drop decreases; if  $\Theta = \pi/2$ , the drops repel and the separation increases. In both cases, after short initial transient, the relative velocity becomes nearly constant and  $d$  changes linearly in time. In the  $\Theta = 0$ , the growing interference as drops approach leads to a non-monotonic dependence on time of  $U_r$ .

Figure 5 shows the dynamics in the case  $R/S > 1$ . In the  $\Theta = \pi/2$  configuration, the drops attract, as expected by the EHD stresslets flow interactions, and the separation decreases monotonically in time. The  $\Theta = 0$  configuration presents more counterintuitive dynamics. Initially, the drops experience repulsion, as expected by EHD interactions, however this interaction is quickly reversed and drop separation decreases. The attraction is likely of dielectrophoretic origin but why is it important at  $\Theta = 0$  configuration and not  $\Theta = \pi/2$  remains a puzzle. Again, after short initial transient, the relative velocity becomes nearly constant and  $d$  decreases linearly in time.

A comparison between the  $R/S < 1$  and  $R/S > 1$  drop-pair dynamics suggests the drops with  $R/S < 1$  interact more strongly as seen from the higher relative velocity and larger changes in separation. This is likely due to the cooperative action and additive effect of the dipolar and electrohydrodynamic interactions.

The effect of the initial misalignment of the drop pair and the applied field direction is illustrated in Figure 6 with the three-dimensional trajectory of drops in the two canonical cases  $R/S < 1$  and  $R/S > 1$ . The pair dynamics in  $R/S < 1$  shows that drops initially attract along the direction of the electric field and then repel and separate in direction perpendicular to the field. The drops remains in the plane defined by the initial separation vector and the applied field direction, in this case the  $xz$  plane. The transient pairing dynamics is clearly seen in the trajectory in the  $xz$  plane. The angle between the separation vector and the applied field continuously increases and around  $60^\circ$  the interactions change from attractive to repulsive, see Figure 7b). At this point the drops attain minimum separation, and after that the drops move away from each other with velocity that overshoots. At long times the drop pair approaches nearly perpendicular orientation relative to the field direction, where the repulsive DEP and EHD interactions push the drops apart. This “kiss-and-run” dynamics is similar to the one observed with ideally polarizable spheres (Saintillan 2008) and has implications to electrocoalescence since the switching from attraction to repulsion prevents drops from reaching proximity sufficient to initiate merger.

In the  $R/S > 1$  case, the drops quickly deform into prolate ellipsoids, attract and move along the field direction and the pair-axis rotates to align almost perpendicularly to the field, see Figure 7b. This “swimming” dynamics is counter the behavior expected from a purely dipolar interaction, which predicts that drops will align with the field. Intriguingly the radial velocity is always positive, indicating attractive interactions (see Figure 7c), while the tangential velocity changes sign consistent with reversal in the direction of motion to upward swim. The behavior likely arises from strong hydrodynamic attraction between the “pusher”-type stresslets. Initially, the second drop is pulled down and towards drop 1, and after that both drops rise and slowly get closer. The swimming can be understood from the stresslet picture: a drop translates in response to the flow by

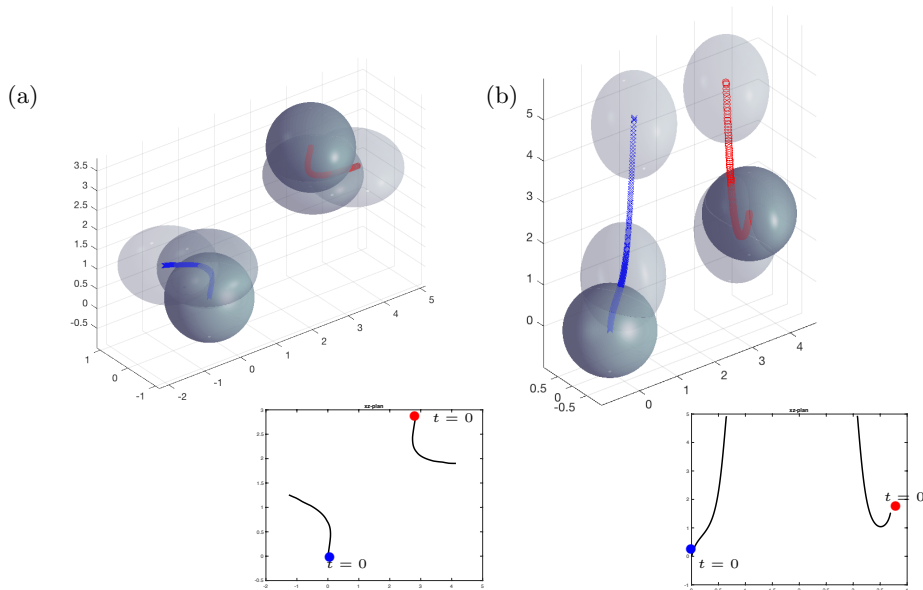


FIGURE 6. Trajectories of two identical drops with  $S=1$  and a)  $R=0.1$  and b)  $R=3$ . Initially the drops are in the  $xz$  plane, the separation in both cases is  $d = 4$  and the angle with the applied field direction is a)  $\Theta = \pi/4$  and b)  $\Theta = 3\pi/8$ . Capillary number  $Ca = 0.5$ . Bottom: trajectories in the  $xz$  planes.

another drop. The translation in a direction making an angle  $\Theta$  with their line of centers can be estimated from the stresslet approximation to be  $\sim V \cos \Theta$ . In this case, this hydrodynamic interaction results in drop drift in the same direction. For the duration of the swimming, drop shapes remain nearly constant, with deformation parameter close to the value predicted by the small deformation theory.

#### 4. Conclusions and outlook

We develop a numerical method, based on the boundary integral formulation of the leaky dielectric model, to study the three-dimensional electrohydrodynamic interactions of a drop pair. We present results for the case of a uniform electric field and arbitrary angle between the drops line of centers and the applied field direction, where the non-axisymmetric geometry necessitates three-dimensional simulations.

The dynamics of drops with  $R/S < 1$  is similar to ideally-polarizable spheres (Saintillan 2008) due to the similarities of the flow pattern and the cooperative action of the dipolar and electrohydrodynamic interactions. If the drops are aligned with the field, the electrostatic attraction and the electrohydrodynamic flow pull the drops towards each other, while the drops are pushed apart if aligned perpendicularly to the field. The critical angle for the reversal of the initial interaction (upon application of the field), from attractive to repulsive, can be estimated from the far-field electrostatic and flow fields, due to a point-dipole and stresslet, respectively. Our study finds that if the drop-pair angle with the field initially is close to the critical angle for reversal, the drops do not experience monotonic attraction or repulsion; instead they attract and move in the di-

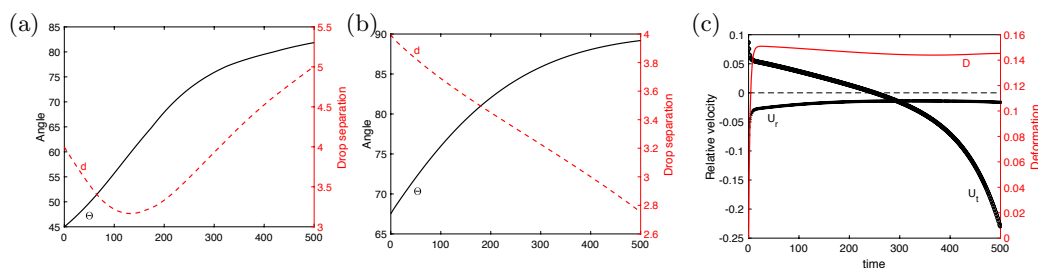


FIGURE 7. Dynamics of the pair of identical drops with  $S = 1$  placed at initial distance  $d = 4$  and initial inclination of  $\Theta = \pi/4$ ,  $R=0.1$  (a), and  $\Theta = 3\pi/8$ ,  $R=3$  (b). Time evolution of the angle between the line of centers of the drops and the applied field direction and the center-to-center distance between the drops. (c) Radial and tangential components of the relative velocity, and deformation of drop 1 for the  $R=3$  drops.

rection of the field and then separate in the transverse direction. Hence, coalescence will be prevented in such case.

In the case of  $R/S > 1$  the dipolar and stresslet flow interactions are antagonistic. The dependence on distance and  $R$  of the competing electrostatic and electrohydrodynamic interactions leads to more complex pair dynamics compared to drops with  $R/S < 1$ . While the latter can be understood by approximating the drops as point-dipoles and stresslets, this picture appears to be an oversimplification in the case of  $R/S > 1$ . The non-trivial dynamics for  $R/S > 1$  will be investigated in detail in a forthcoming study.

Our three-dimensional boundary integral method is also capable of simulating the dynamics of dissimilar drops (different size, viscosities,  $R$  and  $S$ ), and many drops, which we plan to explore in the future.

## 5. Acknowledgments

CS gratefully acknowledges support by Comsol Inc. PV has been supported in part by NSF award CBET 1704996.

## REFERENCES

- ANAND, V., ROY, S., NAIK, VIJAY M., JUVEKAR, VINAY A. & THAOKAR, ROCHISH M. 2019 Electrocoalescence of a pair of conducting drops in an insulating oil. *J. Fluid. Mech.* **859**, 839–850.
- BAYGENTS, J. C., RIVETTE, N. J. & STONE, H. A. 1998 Electrohydrodynamic deformation and interaction of drop pairs. *J. Fluid. Mech.* **368**, 359–375.
- BROSSEAU, Q. & VLAHOVSKA, P. M. 2017 Streaming from the equator of a drop in an external electric field. *Phys. Rev. Lett.* **119**, 034501.
- CASAS, P. S., GARZON, M., GRAY, L. J. & SETHIAN, J. A. 2019 Numerical study on electrohydrodynamic multiple droplet interactions. *Phys. Rev. E* **100**, 063111.
- COLLINS, R. T., JONES, J. J., HARRIS, M. T. & BASARAN, O. A. 2008 Electrohydrodynamic tip streaming and emission of charged drops from liquid cones. *Nature Physics* **4**, 149–154.
- COLLINS, R. T., SAMBATH, K., HARRIS, M. T. & BASARAN, O. A. 2013 Universal scaling laws for the disintegration of electrified drops. *PNAS* **110**, 4905–4910.
- DONG, QINGMING & SAU, AMALENDU 2018 Electrohydrodynamic interaction, deformation, and coalescence of suspended drop pairs at varied angle of incidence. *Phys. Rev. Fluids* **3**, 073701.

- EOW, J. S. & GHADIRI, M. 2002 Electrostatic enhancement of coalescence of water droplets in oil: a review of the technology. *Chem. Eng. Sci.* **85**, 357–368.
- GANAN-CALVO, A. M., LOPEZ-HERRERA, J. M., REBOLLO-MUNOZ, N. & MONTANERO, J. M. 2016 The onset of electrospray: the universal scaling laws of the first ejection. *Scientific reports* **6**, 32357.
- HA, J. W. & YANG, S. M. 2000 Electrohydrodynamics and electrorotation of a drop with fluid less conductive than that of the ambient fluid. *Phys. Fluids* **12**, 764–772.
- KARYAPPA, RAHUL B., DESHMUKH, SHIVRAJ D. & THAOKAR, ROCHISH M. 2014 Breakup of a conducting drop in a uniform electric field. *J. Fluid Mech.* **754**, 550–589.
- KENNEDY, CHRISTOPHER A. & CARPENTER, MARK H. 2003 Additive runge–kutta schemes for convection–diffusion–reaction equations. *Applied Numerical Mathematics* **44** (1), 139 – 181.
- LAC, E. & HOMSY, G. M. 2007 Axisymmetric deformation and stability of a viscous drop in a steady electric field. *J. Fluid. Mech* **590**, 239–264.
- LIN, YUAN, SKJETNE, PAAL & CARLSON, ANDREAS 2012 A phase field model for multiphase electro-hydrodynamic flow. *International Journal of Multiphase Flow* **45**, 1 – 11.
- MELCHER, J. R. & TAYLOR, G. I. 1969 Electrohydrodynamics - a review of role of interfacial shear stress. *Annu. Rev. Fluid Mech.* **1**, 111–146.
- MHATRE, SAMEER, DESHMUKH, SHIVRAJ & THAOKAR, ROCHISH. M. 2015 Electrocoalescence of a drop pair. *Physics of Fluids* **27** (9), 092106.
- DE LA MORA, J. F. 2007 The fluid dynamics of taylor cones. *Ann. Rev. Fluid. Mech.* **39**, 217–243.
- ROY, S., ANAND, V. & THAOKAR, ROCHISH M. 2019 Breakup and non-coalescence mechanism of aqueous droplets suspended in castor oil under electric field. *J. Fluid. Mech.* **878**, 820–833.
- SAINTILLAN, DAVID 2008 Nonlinear interactions in electrophoresis of ideally polarizable particles. *Phys. Fluids* **20** (6).
- SALIPANTE, P. F. & VLAHOVSKA, P. M. 2010 Electrohydrodynamics of drops in strong uniform dc electric fields. *Phys. Fluids* **22**, 112110.
- SALIPANTE, P. F. & VLAHOVSKA, P. M. 2013 Electrohydrodynamic rotations of a viscous droplet. *Phys. Rev. E* **88**, 043003.
- SAVILLE, D. A. 1997 Electrohydrodynamics: The Taylor-Melcher leaky dielectric model. *Annu. Rev. Fluid Mech.* **29**, 27–64.
- SENGUPTA, RAJARSHI, WALKER, LYNN M. & KHAIR, ADITYA S. 2017 The role of surface charge convection in the electrohydrodynamics and breakup of prolate drops. *J. Fluid Mech.* **833**, 29–53.
- SORAGENTONE, C. & TORNBORG, A.-K. 2018 A highly accurate boundary integral equation method for surfactant-laden drops in 3D. *J. Comp. Phys.* **360**, 167–191.
- SORAGENTONE, C., TORNBORG, A.-K. & VLAHOVSKA, PETIA M. 2019 A 3D boundary integral method for the electrohydrodynamics of surfactant-covered drops. *J. Comp. Phys.* **389**, 111–127.
- STONE, H. A., STROOCK, A. D. & AJDARI, A. 2005 Engineering flows in small devices: Microfluidics toward a lab-on-a-chip. *Annu. Rev. Fluid Mech.* **36**, 381–411.
- TAYLOR, G. I. 1966 Studies in electrohydrodynamics. I. Circulation produced in a drop by an electric field. *Proc. Royal Soc. A* **291**, 159–166.
- VLAHOVSKA, PETIA M. 2019 Electrohydrodynamics of drops and vesicles. *Annu. Rev. Fluid Mech.* **51**, 305–330.
- ZABARANKIN, MICHAEL 2020 Small deformation theory for two leaky dielectric drops in a uniform electric field. *Proc. Royal Soc. A* **476** (2233).